Free Electron Laser Ablation of Urinary Calculi: An Experimental Study

Kin Foong Chan, *Member, IEEE*, Bernard Choi, Gracie Vargas, Daniel X. Hammer, *Member, IEEE*, Brian Sorg, T. Joshua Pfefer, Joel M. H. Teichman, Ashley J. Welch, and E. Duco Jansen

***Abstract*—Infrared laser ablation of urinary calculi was investigated as a function of wavelength to determine the relation of ablation threshold fluences, ablation depths, and optical absorption. A simple photothermal ablation model was employed to examine this relationship.**

Human urinary calculi composed of >95% uric acid, >95% cystine, >95% calcium oxalate monohydrate (COM), and >90% magnesium ammonium phosphate hexahydrate (MAPH) were used. Various wavelengths between 2.1 and 6.5 μm were selected to perform threshold fluence and ablation depth measurements. The laser source for this study was the tunable pulsed infrared free electron laser (FEL) at Vanderbilt University.

Experimental results indicated a correlation of threshold fluence and ablation depth to the optical absorption properties of the calculi. When calculus optical absorption increased, the threshold fluences decreased. Although the ablation depths increased with calculus optical absorption, results indicated that in certain calculi the ablation depth was affected by optical attenuation through the ablation plume. These observations were in agreement with the photothermal ablation model, but fractures in striated calculi at higher optical absorptions indicated the contribution of a photomechanical mechanism.

Threshold fluences and ablation depths are a function of the wavelength dependent absorption properties of the calculi. These observations suggest that the 3-μm and 6-μm absorption bands are optimal for ablation or fragmentation of urinary calculus.

***Index Terms*—Absorption, fluence, fragmentation, infrared, kidney stone, lithotripsy, radiant exposure, thermal, urology.**

Manuscript received May 22, 2001; revised October 30, 2001. This work was supported in part by the Office of Naval Research Free Electron Laser Biomedical Science Program under Grant N00014-91-J-1564, UT Austin, and Grant N00014-99-1-10779, Vanderbilt University, the Air Force Office of Scientific Research through MURI from DDR&E under Grant F49620-98-1-0480, UT Austin, in part by the Albert W. and Clemmie A. Caster Foundation (UT Austin), the Air Force Office of Scientific Research under Grant F49620-98-1-0210, UTHSCSA, and in part by the SPIE Educational Scholarship Committee in Optical Science and Engineering (UT Austin).

K. F. Chan was with the Department of Electrical and Computer Engineering, University of Texas, Austin TX 78712 USA. He is now with Ball Semiconductor, Allen, TX 75013 USA.

B. Choi was with the Biomedical Engineering Program, University of Texas, Austin, TX 78712 USA. He is now with the Beckman Laser Institute, University of California, Irvine, CA 92612 USA.

G. Vargas is with the Biomedical Engineering Program, University of Texas, Austin, TX 78712 USA.

D. X. Hammer was with the Department of Electrical and Computer Engineering, University of Texas, Austin, TX 78712 USA. He is now with Physical Sciences, Andover, MA 01810 USA.

B. Sorg was with the Biomedical Engineering Program, University of Texas, Austin, TX 78712 USA. He is now with Duke University Medical Center, Durham, NC 27710 USA.

T. J. Pfefer was with the Biomedical Engineering Program, University of Texas, Austin, TX 78712 USA. He is now with the U.S. Food and Drug Administration Center for Devices and Radiological Health, Rockville, MD 20850 USA.

J. M. H. Teichman is with the Division of Urology, Department of Surgery, University of Texas Health Science Center, San Antonio, TX 78229 USA.

A. J. Welch is with the Department of Electrical and Computer Engineering and the Biomedical Engineering Program, University of Texas, Austin, TX 78712 USA.

E. D. Jansen is with the Department of Biomedical Engineering, Vanderbilt University, Nashville, TN 37235 USA (e-mail: duco.jansen@vanderbilt.edu).

Publisher Item Identifier S 1077-260X(01)11240-2.

I. Introduction

INTERVENTIONAL treatments of urinary calculi have improved drastically over the past two decades. By the early 1990s, four major lithotripsy modalities have been used clinically to remove urinary or renal calculi. They include electrohydraulic lithotripsy (EHL), ultrasonic lithotripsy, extracorporeal shockwave lithotripsy (ESWL) and laser lithotripsy [1]. Each of these modalities has its limitations. EHL, which uses shockwaves induced by electrical discharges, is only suitable for fragile calculi and may cause perforation of the ureter and adjacent tissue. Ultrasonic lithotripsy has been shown to be effective for the removal of both ureteral and renal calculi, but the 11.5 French ureteroscope that must be used to deliver the large ultrasonic probe (6 French) restricts its use to the lower ureter(s). ESWL has the advantage of being performed outside the body, and therefore is a noninvasive procedure. However, visualization of the calculus during the procedure is limited and renal injury may occur. Laser lithotripsy allows the use of small-diameter catheters, which provide access to both ureteral and renal calculi. This technique has also been shown to reliably remove calculi with minimal damage to healthy tissue without the use of ureteroscopy.

Laser ablation was introduced into clinical lithotripsy during the mid-1980s [2]–[5]. The ablation or fragmentation of urinary calculi during that period was achieved with a flashlamp pumped pulsed-dye laser delivered through an optical fiber. Fragmentation occurred due to shockwaves generated as a result of plasma expansion and cavitation bubble collapse [6], [7]. By 1996, the Holmium : YAG laser had become popular not only in lithotripsy but also in other urologic procedures such as laser resection of the prostate. The holmium laser reduced the calculus to passable size by ejecting fine particles from and producing well-demarcated craters on the calculus surface. Several investigators observed that the fragmentation mechanism of urinary calculi by the holmium laser was suggestive of a photothermal process [8], [9].

Two critical factors required for the acceptance of a laser medical procedure involving ablation are 1) maximizing ablation efficiency while 2) minimizing damage to surrounding

healthy tissue. To achieve this, the physical processes of laser ablation must be understood. Unfortunately, these processes are complicated. Previous studies indicate that the physical mechanism is a function of laser parameters and physical properties of the material to be ablated [10]. Some researchers have shown that laser pulse duration determines whether an ablation process is predominantly photothermal or photoacoustical [10], [11]. Izatt *et al.* [12] and more recently Nahen *et al.* [13] have explored the effect of debris screening during a laser pulse upon ablation efficiency. Walsh and Cummings [14], and Jansen *et al.* [15] have examined the dependence of optical absorption upon temperature at 2.94 and 1.96 μm, and how dynamic changes in absorption affect the outcome of the ablation process. The roles of tissue mechanical properties such as tensile strengths and viscosity on ablation have also been explored [16]–[18].

Because of the many advantages of the mid-infrared holmium laser over the flashlamp pumped pulsed-dye laser in clinical lithotripsy, researchers have pondered over the most efficient wavelengths for such a procedure. However, the role of wavelength dependent optical absorption and its effect on urinary calculi ablation has not been extensively studied. Daidoh *et al.* [19] have suggested that 3 and 6 μm may be the optimum wavelengths for ablating calcium oxalate monohydrate (COM) and uric acid calculi because of their peak absorptions. Unfortunately, these authors did not introduce a sound theoretical or physical basis for their postulation. In a recent study of the dominant ablation mechanism in long-pulsed Ho : YAG laser lithotripsy [9], [20], we observed that the holmium laser-calculus ablation dynamics are comparable to several previous studies of hard-tissue laser ablation [12], [21]. A photothermal ablation model was used in these studies to analyze the experimental results [12], [21]–[24]. We hypothesize that the optimal wavelength(s) in the infrared spectrum for calculus ablation is highly dependent upon the optical absorption properties as specified by the value of the absorption coefficient μ_a (mm^{-1}). The optimal wavelength can be defined as the wavelength at which ablation efficiency, as measured in terms of mass-loss/Joule (mg/J), or ablation depth/Joule (μm/J), etc., is the highest relative to other achievable laser wavelengths.

Most urinary calculi strongly absorb infrared energy from 2 to 10 μm with relatively low scattering. Acoustic velocities in the dense crystal structures of urinary calculi are similar to or higher than the speed of sound in water ($\sigma \sim 1520$ m/s) [24]. Thus, for highly absorbed wavelengths that are used for ablative purposes, microsecond or longer laser pulses are not stress confined, and therefore do not cause fragmentation by means of shock waves as do submicrosecond laser pulses. When the process is not stress confined, ablation becomes dominated by photothermal mechanisms such as vaporization, melting, and chemical decomposition [20], [24]. A simple model introduced by Olmes *et al.* [23] for determining the threshold fluence, $H_{\rm th}$ (J/cm^2), for thermal ablation can be expressed as

$$H_{\rm th} = \frac{1}{\mu_a}\left[\rho c(T_{\rm th} - T_o) + L\rho\right] = \frac{W_{\rm abl}}{\mu_a} \tag{1}$$

where μ_a (cm^{-1}) is the optical absorption coefficient of the calculus, ρ (kg/m^3) is the calculus density, c (J/g.K) is the specific heat, $T_{\rm th}$ is the threshold temperature for vaporization, melting, or chemical decomposition, T_o is the ambient temperature, L (J/g) is the latent heat for vaporization, melting, or chemical decomposition, and $W_{\rm abl}$ is the heat of ablation (J/cm^3). Assuming that the calculus density, specific heat, and threshold temperature are constants, the heat of ablation is also a constant thermal property of a particular calculus type. The predicted dependence of the threshold fluence $H_{\rm th}$ on the calculus optical absorption as a function of the heat of ablation is illustrated in Fig. 1 for three values of the heat of ablation, where $W_{\rm abl1} < W_{\rm abl2} < W_{\rm abl3}$.

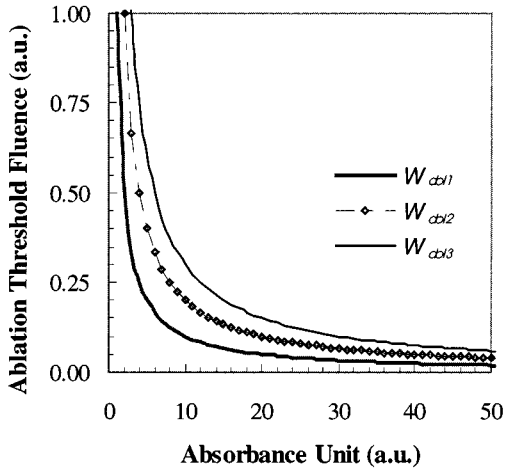

Fig. 1. Prediction of the relationship between ablation threshold fluence and absorbance for some hypothetical tissues with different heat of ablation, $W_{\rm abl}$. In this case, $W_{\rm abl3} > W_{\rm abl2} > W_{\rm abl1}$.

The photothermal ablation model used in this study has been derived by previous researchers for ablation studies in dentine and beef shank bone [23], [25]–[27]. During the period of no heat conduction, the ablation depth d (μm) is

$$d = \frac{1}{\gamma}\ln\left[\frac{\gamma}{\mu_a}\left(\frac{H}{H_{\rm th}} - 1\right) + 1\right] \tag{2}$$

where γ is the intrapulse debris attenuation coefficient (cm^{-1}), and H is the incident laser fluence (J/cm^2). Detailed derivation of (2) is discussed elsewhere [28], [29]. Ostertag *et al.* and Hibst *et al.* [25], [26] have verified this model in their studies of dentine ablation depth as a function of incident laser fluence. Izatt *et al.* [30] has attempted to apply this ablation model to interstitial water vaporization and expansion for extracting the optical properties of beef bone shank.

If multiple laser pulses are employed to achieve sufficient ablation depth for accurate measurement, and if one pulse does not affect the result of the next pulse, then the total ablation depth is

$$d = \sum_{n=1}^{i}\left\{\frac{1}{\gamma}\ln\left[\frac{\gamma}{\mu_a}\left(\frac{H_n}{H_{\rm th}} - 1\right) + 1\right]\right\} \tag{3}$$

where H_n is the laser fluence of individual pulses for a total of i pulses. Equation (3) assumes the laser pulses do not overlap in time, and that successive pulses are sufficiently far apart in time that debris screening from a previous pulse does not affect the next pulse. Pulse-to-pulse variation in material optical and thermal properties would affect the accuracy of (3) where we assume constant parameters. We have extended the theoretical

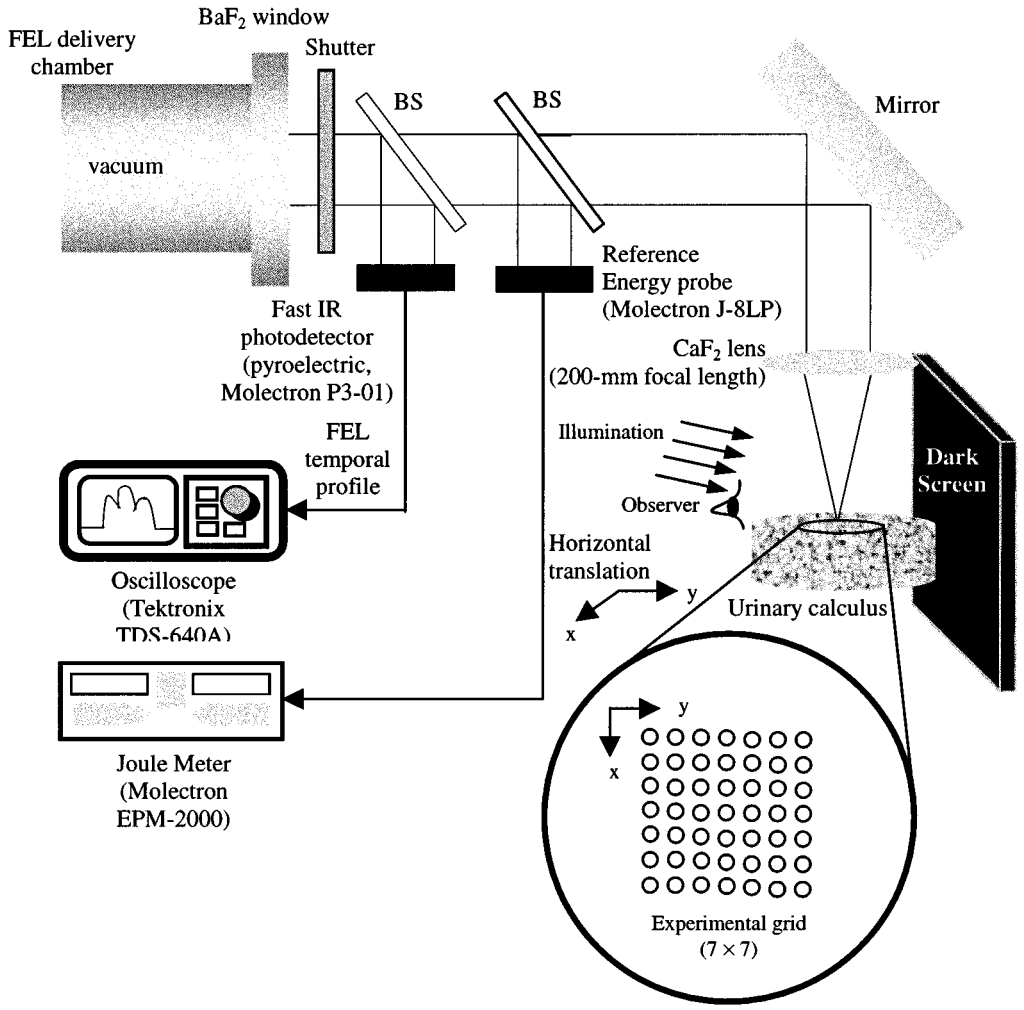

Fig. 2. Experimental setup for measuring the threshold fluences and ablation depths. BS: Beam splitter.

model to evaluate the dependence of the ablation depth on the optical properties of the urinary calculi and ejected particles in the infrared wavelengths using the free electron laser. By understanding the ablation dynamics, and calculus optical properties it may be possible to determine the optimum wavelength for fragmentation.

The objectives of this study are: 1) to investigate the mechanism(s) involved in urinary calculus ablation; and 2) to determine the threshold fluences for ablation H_{th}, and the corresponding ablation depths d, and to examine their correlation with optical absorption. The most common human urinary calculi are used in this *in vitro* study in which their optical absorption properties are known, for the purpose of investigating the physical dynamics involved in the ablation process as well as addressing their relevance for future clinical studies. Experimental observations and deviations from (1) and (3) are used to determine the contribution of other physical mechanisms and dynamic properties involved in the ablation processes.

II. Materials and Methods

A. Calculus Specimen

Four types of human urinary calculi were used in this experiment. These calculi were composed of, respectively, >95% uric acid, >95% cystine, >95% calcium oxalate monohydrate (COM), and >90% magnesium ammonium phosphate hexahydrate (MAPH) and were obtained from a calculus analysis laboratory (Louis C. Herring Company, Orlando, FL). The calculi were cut with a diamond saw, producing samples 2–3 mm in thickness with flat (approximately parallel) surfaces. After cutting, the calculi were dehydrated in a lyophilizer and stored in sample container with room air until the time of use.

B. Laser Source and Delivery

The pulsed infrared Free Electron Laser (FEL) at Vanderbilt University, which is tunable from 2.1 to 9.8 μm, was used for this experiment. The FEL macropulses ($\tau_p \sim 3$–5 μs FWHM) consisted of a sequence of 1-ps micropulses with a 350-ps interpulse interval. Hence, one macropulse had approximately 8550 to 14 250 micropulses. The FEL had a Gaussian beam profile, exhibiting laser emission with the TEM_{00} mode. These were the characteristic pulse structures and properties of the FEL at Vanderbilt University. Although it was not known if individual picosecond micropulses might contribute to fragmentation, the short macropulse duration ensured thermal confinement in highly absorbing specimens demonstrated in all previous and current clinical laser lithotripsy modalities.

Single pulses were used for threshold measurements, whereas a repetition rate of 5 Hz was used for ablation rate measurements. Wavelengths used in this experiment were 2.12, 2.50, 2.94, 3.13, 3.21, 3.62, 4.00, 4.57, 4.74, 4.77, 5.00, 5.60, 5.99, 6.04, 6.17, 6.20, 6.26, 6.29, 6.31, and 6.45 μm. The 2.12 and 2.94 μm wavelengths correspond to the wavelengths for the Ho : YAG laser and Er : YAG laser, respectively, and served as references for comparison to results from commercial lasers. Wavelengths were chosen to correspond to the peaks, inclinations, and valleys within the infrared absorption spectra of individual calculus types referenced from Dao and Daudon [31] and Daidoh *et al.* [19]. The absorption spectra from these references are in relative optical absorbance units (a.u.) and not absolute values of absorption coefficients (cm^{-1}).

The experimental setup for the measurement of threshold fluence and ablation depth is illustrated in Fig. 2. The FEL beam was delivered via a vacuum beam transport system, and reached our setup through a BaF_2 window. A footswitch-controlled mechanical shutter blocked the laser beam. When the shutter was opened, the laser beam was delivered to the urinary calculus via a 2-in diameter, 200-mm focal length CaF_2 lens. The FEL beam is linearly polarized and the pulse energy was adjusted by rotating a double Brewster plate polarizer located within the vacuum chamber. A fast infrared (IR) photodetector (pyroelectric, Molectron P3-01, Portland, OR) was used to monitor the temporal profile of the laser pulse on a digital oscilloscope (Tektronix TDS 640A, Beaverton, OR). Two energy probes (Molectron J-8LP, Portland, OR) were used prior to the experiment to measure the energy ratio (correction factor = output energy/reference energy). During each experiment, only the reference energy was recorded and was scaled afterwards according to the correction factor. For each wavelength, the spot diameter of the incident laser beam was measured at the focal point using a standard knife-edge technique [32]. The FEL spatial beam profile was approximately Gaussian [33]. The FEL spot diameter used was 210 $\pm$10 μm. The sample calculus was mounted on a manual precision x–y translation stage with its top surface aligned orthogonally to the optical axis and at the focal plane. Irradiation sites corresponded to a 7 $\times$ 7 grid (i.e., maximum data points, $n = 49$, grid spacing = 1 mm). Post-experimental calculation of the incident laser fluence was performed by dividing the corrected incident laser energy by the measured spot area based on the $1/e^2$ diameter.

C. Ablation Threshold Fluence

The threshold fluence $H_{\rm th}$ for ablation was defined as the incident laser fluence required to produce mass ejection from the urinary calculus. A single-shot laser pulse was gated (by opening the shutter) to each point on the 7 $\times$ 7 grid. A double-blind study was conducted in which an operator altered the pulse energy level around the anticipated threshold. The observer was alerted before the operator gated a pulse to the calculus and each pulse was scored as a 1 (mass ejection) or a 0 (no mass ejection). Visual detection of plume formation was aided with forward illumination and a dark background as depicted in Fig. 2. No visual magnification was used. The double-blind study prevented biased decisions. Post-experimentally, results were analyzed using *Probit* analysis [34] (Fig. 3). The threshold fluence, $H_{\rm th}$, was specified as the laser fluence at which ablation occurred with a 50% probability, ED_{50}. ED_{63} and ED_{37} were used as the upper and lower limits of the experimental error, respectively. This probabilistic approach was taken to account for localized variations in the optical, thermal, and mechanical properties of a specimen that might have affected the threshold fluence values for ablation.

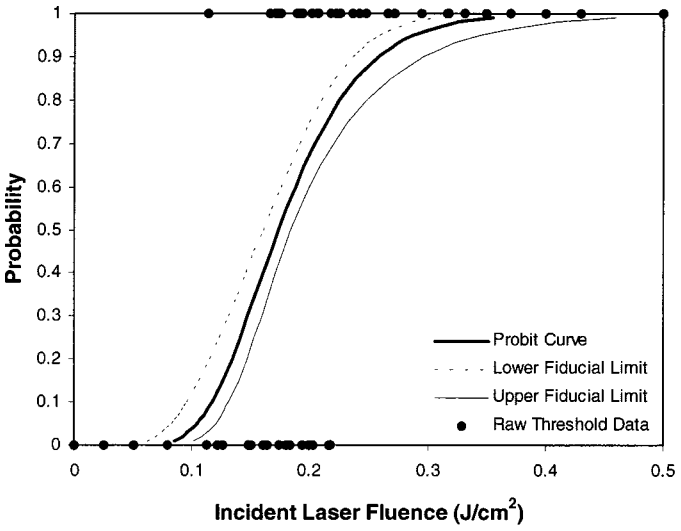

Fig. 3. A *probit* curve for uric acid calculus irradiated at 3.13 μm. The probit curve determines the probability of ablation given a range of incidence laser fluences (J/cm^2). The fiducial limits, which express the confidence interval, were set at 63% ($1/e$) for all of our calculations. The threshold fluence is defined as the value at which the probability of ablation is 50% (ED_{50}), estimated to be $H_{\rm th} = 0.173$ J/cm^2 in this case. We set the lower and upper bounds of experimental errors at 37% (ED_{37}) and 63% (ED_{63}) probability for ablation, respectively, for all data points shown in Fig. 4. • represents the raw threshold data points ($n = 45$) recorded during the experiment. ED: estimated dose.

D. Ablation Depth

For each calculus type, two cut samples from the same parent calculus were used. At each wavelength, ten ablation craters were made ($n = 10$). Each crater was produced by a fixed fluence of 5 J/cm^2 per pulse for a total of 10 pulses (or a total fluence of 50 J/cm^2) gated to the calculus surface at a 5-Hz repetition rate. The slow repetition rate was used to minimize interpulse debris screening which was determined using fast-flash photography [9], by estimating the period from laser onset to when ejected particles have left the optical axis of the laser beam (typically <10 ms). Post-experimentally, the ablation depths d were measured under a 112.5$\times$ surgical microscope (Nikon SMZ-U, Melville, NY) by measuring the displacement in the focal plane between the crater surface and the crater floor using a precision translation stage (MX700 Series Micromanipulators, Siskiyou Design Instruments Inc., Grants Pass, OR). The spatial resolution of this measurement was limited by the depth of focus ($\sim$20 μm) of the microscope lens.

A CCD camera (HV-C20, Hitachi, Tokyo, Japan) and an optical coherence tomography (OCT) system were used to acquire images for qualitative post-ablation analyzes. The CCD images were used to compare the surface effects on the calculi produced by ablation at different wavelengths. OCT images (spatial reso-

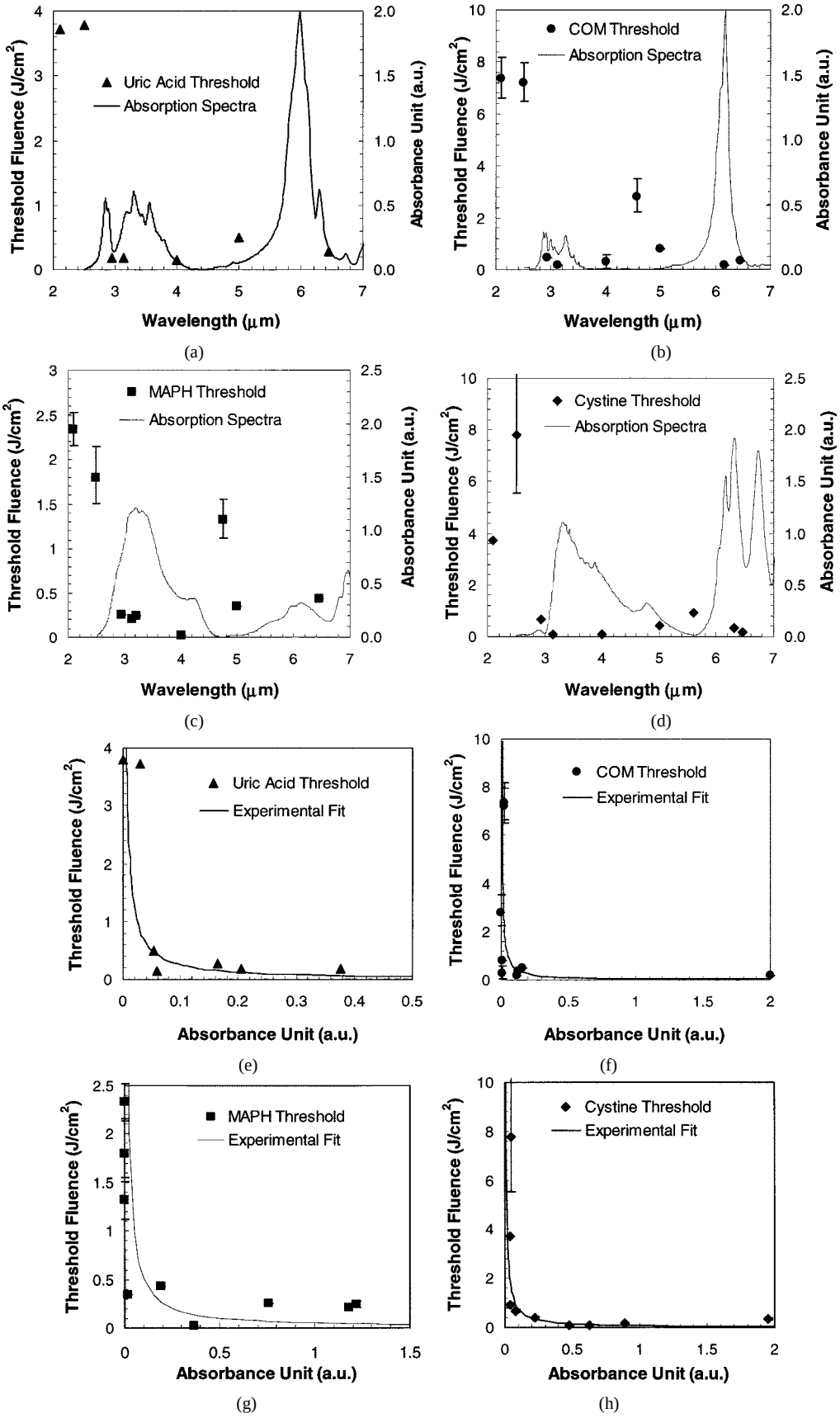

Fig. 4. Ablation threshold fluences (J/cm^2) versus wavelength (μm) for (a) uric acid, (b) COM, (c) MAPH, and (d) cystine urinary calculi. The absorption spectra of individual calculus types in unit absorbance, referenced from Dao and Daudon [31], are superimposed for comparison. In (e)–(h), the threshold fluences are plotted as a function of absorbance unit for the corresponding calculus types. An experimental fit indicates that the measured threshold fluences are in good agreement with (1). A maximum of 49 data points were recorded with varying laser fluences around the threshold, each with a single pulse. Error bars indicate the ED_{37} and ED_{63} values obtained from probit analysis for each data set.

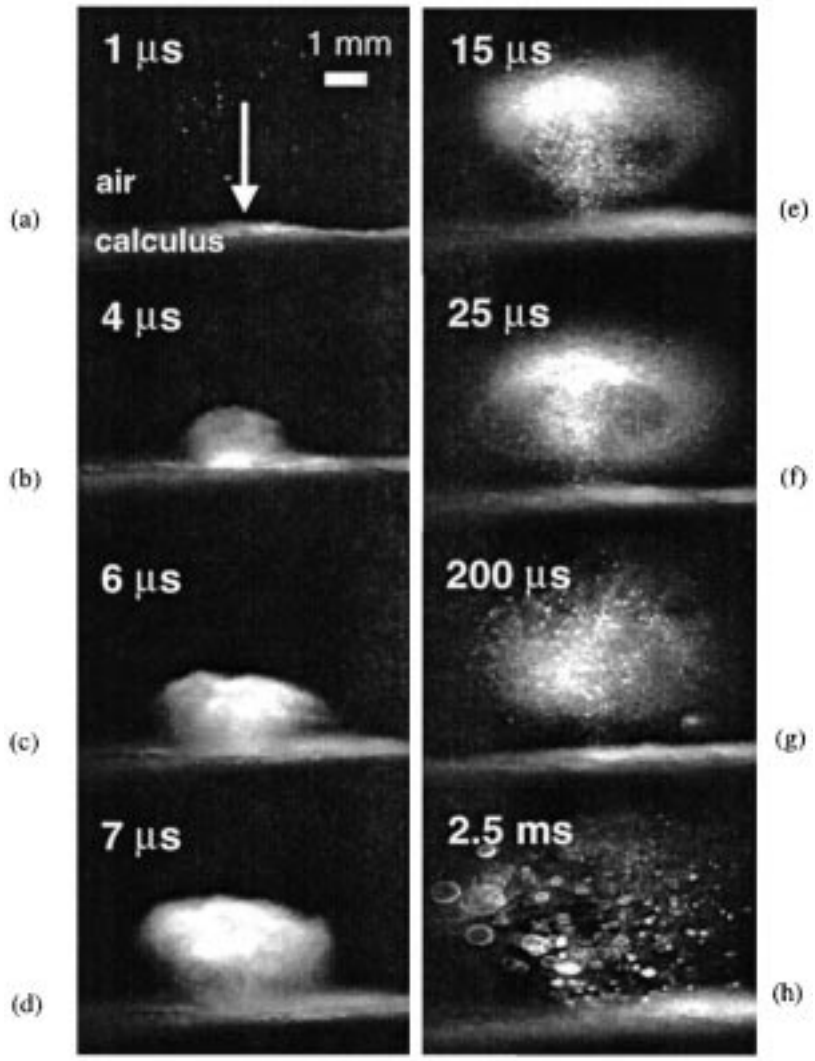

Fig. 5. Dynamics of ablation on a COM calculus. Within 1 μs after laser onset, (a) debris was seen ejected from the surface at laser impact. At the end of the laser pulse ($\sim$4 μs), (b) the ablation plume continues to expand. It is possible that debris screening may have affected the amount of light absorption within the calculus. By 2.5 ms, (h) most ejected particles were seen as out-of-focus debris, implying a much lower density of particles along the FEL beam path.

lution $\sim$23 μm but better vertical cross-sectional visualization) were used to confirm the ablation depth measurements with the surgical microscope.

III. Results

A. Ablation Threshold Fluence

Results of threshold fluences for ablation are presented in Fig. 4. Fig. 4(a)–(d) shows the threshold fluence as a function of wavelength, with the relative absorption spectra (absorbance unit) of individual calculus types included for qualitative comparison. In general, threshold fluences are higher in regions of low optical absorption for all calculi, and vice versa. When the threshold values are plotted as a function of absorbance unit, the results [Fig. 4(e)–(h)] fit (1). The experimental fit in Fig. 4(e)–(h) is performed by assuming the absorbance unit is in linear proportion to the absorption coefficient in (1), and that the heat of ablation is a constant parameter consisting of fixed thermal properties of each individual calculus type. Error bars, representing the ED37 and ED63, are shown only for errors larger than the size of the data points.

B. Ablation Depth

Pump–probe images (Fig. 5) show that an ablation plume is visible as early as 1 μs after the onset of the 3–5 μs long laser pulse, indicating that plume attenuation might affect the ablation process during the laser pulse duration. In the same figure, it can be seen that by 2.5 ms after the laser onset, most ejected mass was removed from the optical axis away from the beam path. At 10 ms after the onset no remaining debris was visible in the beam path (image not shown). Since the experiment was performed at 5 Hz, the interval between each subsequent pulse was 200 ms—20 times longer than the maximum lifetime of the plume. Hence, it is reasonable to assume that no interpulse debris screening occurred at a pulse repetition rate of 5 Hz.

In general, the ablation depth caused by ten pulses with a fluence (per pulse) of 5 J/cm^2 increases with absorbance or optical absorption (Fig. 6). The ablation depth as a function of laser wavelength in comparison to the absorption spectra of individual calculus types is presented in Fig. 6(a)–(c). When plotted against the absorbance units [Fig. 6(d)–(f)], the results are in fair agreement with (3). The experimental fit in Fig. 6(d)–(f) is

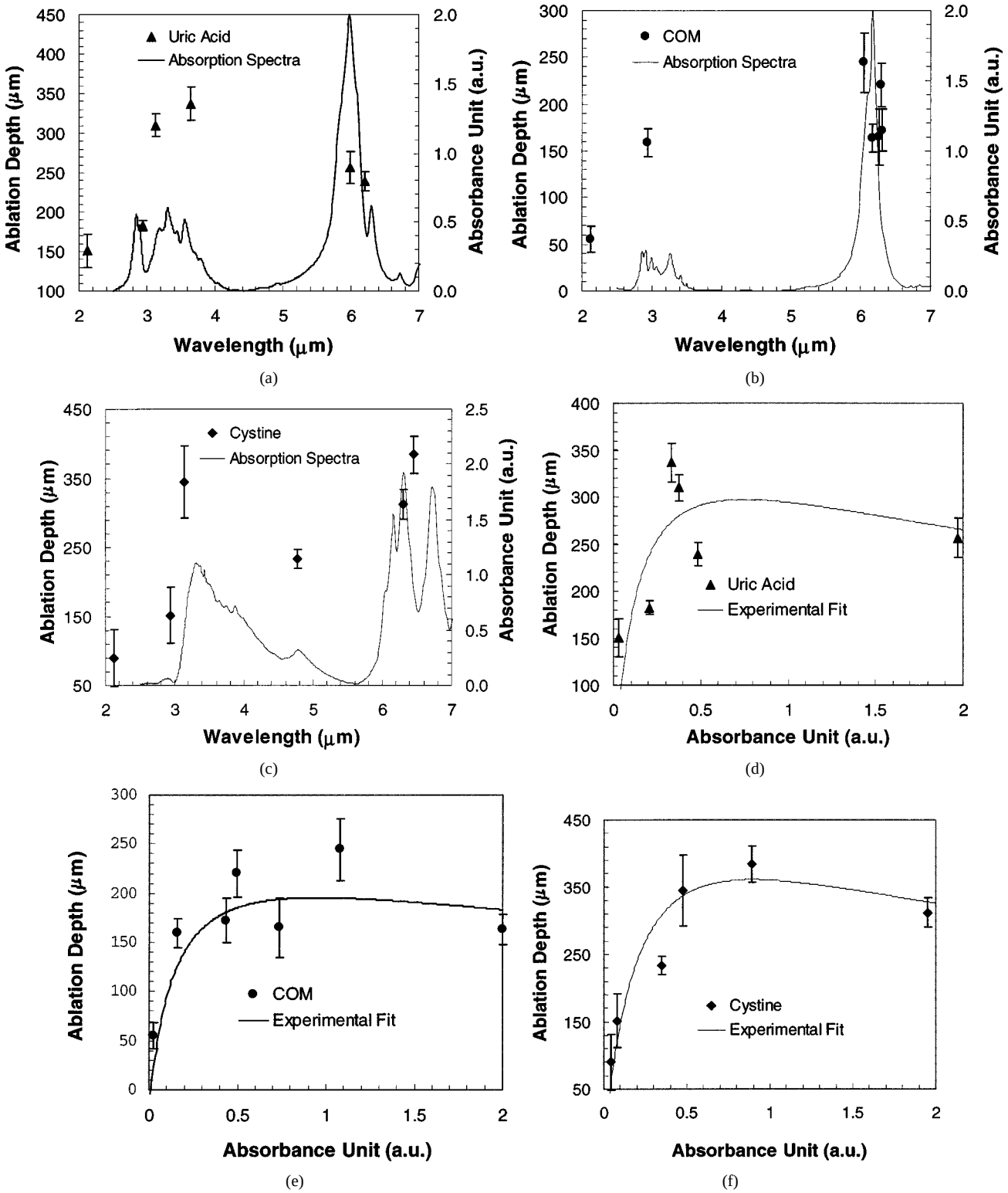

Fig. 6. Ablation depths (μm) versus wavelength (μm) for (a) uric acid, (b) COM, and (c) cystine urinary calculi. The absorption spectra of individual calculus types in unit absorbance, referenced from Dao and Daudon [31], are superimposed for comparison. In (d)–(f), the ablation depths are plotted as a function of absorbance unit for the three types of calculi. An experimental fit indicates that the measured depths are in fair agreement with (3). A total of ten data points ($n = 10$) were collected at each wavelength for each calculus types, with a constant laser fluence of 5 J/cm^2 for a total of 10 pulses at 5 Hz.

performed 1) by assuming the absorbance unit is in linear proportion to the absorption coefficient in (2); 2) with an increasing debris attenuation as a function of increasing absorbance unit; 3) by using the threshold fluence values estimated (experimental fit values) in Fig. 4(e), (f), and (h), respectively; and 4) the experimental value of incidence laser fluence. Ablation depth results for the MAPH calculi are not shown because of insufficient data points. Typical ablation crater vertical cross sections acquired by OCT for uric acid calculi irradiated at 2.12, 2.94, and 5.99 μm are shown in Fig. 7. The ablation depths increase

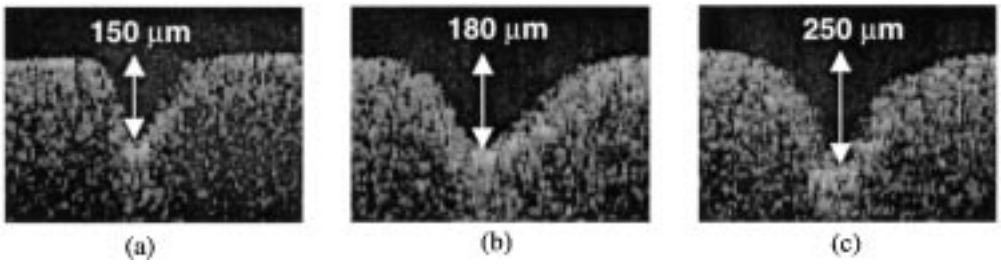

Fig. 7. Effects on ablation depth as a function of increasing optical absorption, respectively, at (a) 2.12 μm, (b) 2.94 μm, and (c) 5.99 μm, on an uric acid calculus. Each ablation crater was irradiated with a total fluence of 50 J/cm^2 (ten pulses at 5 J/cm^2) at 5 Hz. Each vertical cross-sectional ablation crater images was recorded using an OCT system having a longitudinal spatial resolution of 23 μm.

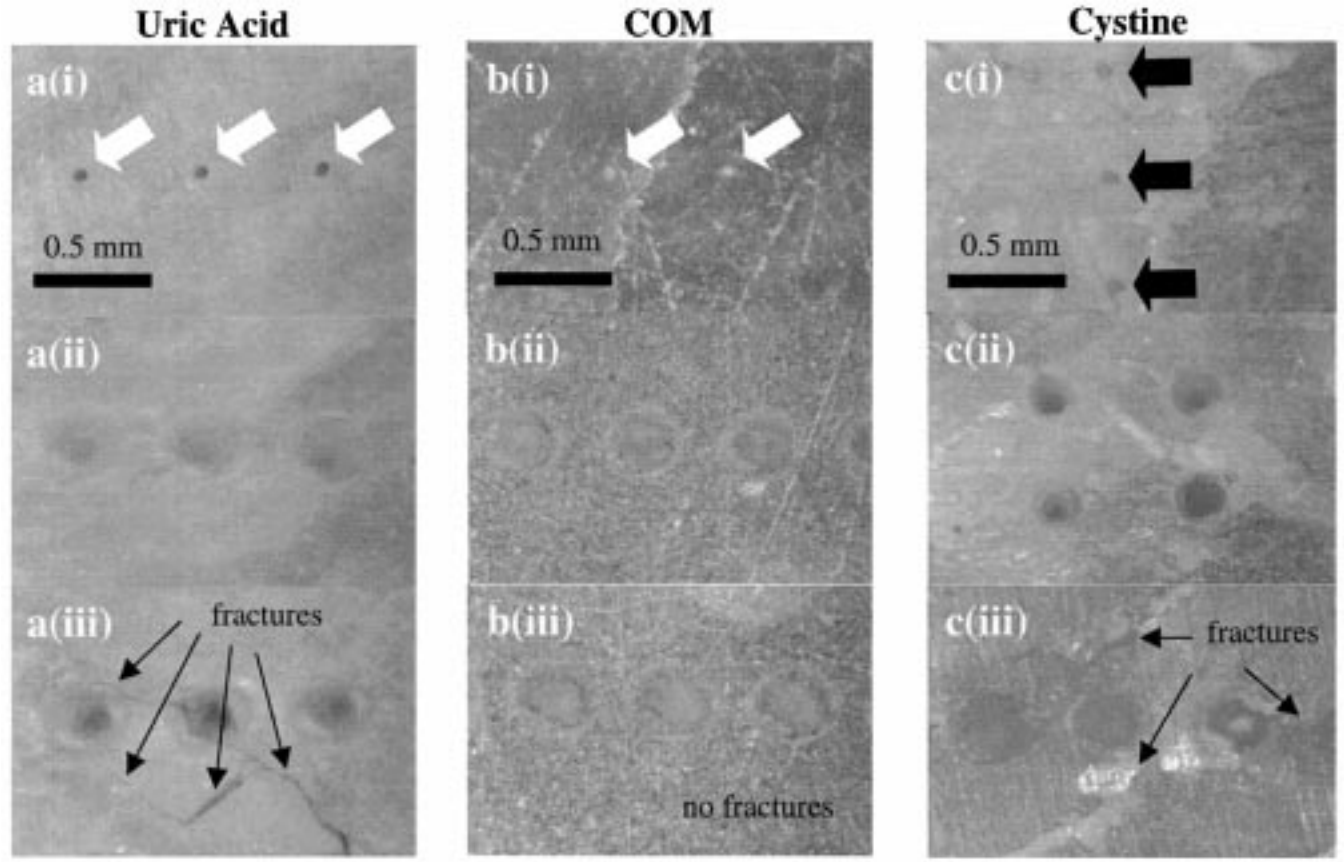

Fig. 8. Examples of surface images of ablation crater of (a) uric acid, (b) COM, and (c) cystine calculi. For each calculus type, the images from top to bottom, (i)–(iii), illustrate the effects of infrared laser ablation as a function of increasing optical absorption (in absorbance unit). Wavelengths used were 2.12 μm (i), 6.20 μm (ii), 5.99 μm (iii) for the uric acid calculus; 2.12 μm (i), 6.04 μm (ii), 6.17 μm (iii) for the COM calculus; and 2.12 μm (i), 3.13 μm (ii), 6.31 μm (iii) for the cystine calculus. Each ablation crater was irradiated with a total fluence of 50 J/cm^2 (10 pulses at 5 J/cm^2) at 5 Hz. Laser spot size was 210 $\pm$ 10 μm. Images were recorded using a surgical microscope (112.5$\times$) and a color CCD camera.

slowly as a function of rising optical absorption in this sequence of OCT images. In all OCT images recorded, no internal fracture (limited to fracture sizes $>$23 μm) is seen surrounding the craters, although debris seems to have remained within some craters. Fig. 8 shows the surface of craters recorded with the surgical microscope (112.5$\times$) and a color CCD camera. The figure shows craters ablated at wavelengths with low absorption to high absorption (in relative absorbance unit) from top to bottom, for various urinary calculi. With a 5-Hz pulse repetition rate, no carbonization indicative of thermal damage around the craters is seen. Surface fractures or adjacent mechanical damage are observed surrounding the craters of uric acid [Fig. 8(a)(iii)], cystine [(Fig. 8(c)(iii)], and MAPH (not shown) calculi at wavelengths with higher relative absorbance. No fracture is apparent surrounding the craters of COM calculi [Fig. 8(b)(i–iii)] at all wavelengths tested.

IV. Discussion

In order to identify the optimal wavelengths and elucidate the ablation mechanism, ablation threshold values and ablation rates for the most common types of human urinary calculi were measured over a broad range of the infrared spectrum. In this study, the measured threshold fluences for ablation in the infrared spectrum are strongly influenced by the optical absorption of the calculi. The experimental results indicate that if calculi are irradiated at wavelengths with higher optical absorption, the laser fluences required to initiate ablation can be significantly reduced [Fig. 4(a)–(d)]. In general, threshold fluences

are proportional to the reciprocal of the absorbance, and thus to the absolute absorption coefficients [Fig. 4(e)–(h)]. These results and (1) suggest that the heat of ablation, W_{abl} is a constant thermal property that is not wavelength dependent. With higher optical absorption, less laser fluence is required to reach the heat of ablation. The excess laser fluence beyond threshold is spent on the removal of calculus mass and progression of the ablation front. The change in ablation depth as a function of absorbance is in fair agreement with this photothermal model [(2)].

For low optical absorptions in all calculus types, ablation depth increased as absorption increased [Fig. 6(d)–(f)]. However, ablation depth was bounded for higher absorption coefficients, and eventually a decrease in ablation depth occurred for even higher optical absorption in uric acid, cystine, and COM calculi [Fig. 6(d)–(f)]. These results are in agreement with (2), which considers attenuation of the laser beam by the ablation plume. The experimental results indicate some plume generation 1 μs after the onset of the laser pulse [Fig. 5(a) and (b)]. When the attenuation coefficient of the ablation plume or debris, γ, is much smaller than the calculus absorption coefficient μ_a, but increases with μ_a, there is a predicted decrease in ablation depth as μ_a becomes large [13], [28], [29]. The bounding of ablation depth at higher optical absorption is consistent with a thermal mechanism but contrary to a process dominated by a photomechanical or photoacoustical mechanism. The photomechanical or photoacoustical mechanism removes calculus by large fragment dissociation [35], whereas the photothermal mechanism removes fine particles and creates well-demarcated craters [36]. The plume contains ejected fragments that absorb and scatter the incident laser beam, thus reducing the amount of energy available for ablation. By performing the ablation at a relatively low repetition rate (5 Hz), interpulse debris screening of consecutive laser pulses was negligible compared to intrapulse debris screening. At higher optical absorption, the debris limits the amount of laser energy available for ablation and ablation depth decreases. In addition, more laser energy may be coupled in acoustic energy that fractures the crater proximity but is not strong enough to cause mechanical ablation [Fig. 8(a)(iii) and (c)(iii)].

We believe the ablated mass from the irradiated calculus volume was removed before significant heat conduction could occur. While no explicit data on the thermal diffusivity of urinary calculi were found in the literature, analysis of data on similar materials such as bone and teeth (enamel and dentin) [37] indicate that thermal confinement is met for absorption depths >2 μm (i.e., $\mu_a < 5000\ \mathrm{cm}^{-1}$). Experimentally, this assumption is supported by the fact that no carbonization to areas surrounding the crater was observed at 5 Hz (Fig. 8).

While threshold fluence data and ablation depth measurements generally followed the predictions from the thermal ablation model, some discrepancies occurred. For example, at 3.13 and 3.64 μm in uric acid calculus [Fig. 6(d)], the ablation depth was much higher than expected, indicating that the actual optical absorption of the calculi used in the experiment deviated from the absorption spectra reported by Dao and Daudon [31]. Striated and irregular appearance of the urinary calculi suggested the presence of impurities (i.e., unknown amorphous organic compounds or crystalline minerals) and inhomogeneities (i.e., regions containing the dominant constituents but at different densities).

Another possibility is that the mechanical integrity of the uric acid molecule may have been compromised by wavelength specific absorption of intramolecular bonds. In this case, the irradiance wavelengths of 3.13 and 3.64 μm are associated with the energy band close to the OH group in the uric acid calculus [19].

Ablation crater images obtained with OCT (Fig. 7) resemble predictions from a two-dimensional ablation model proposed by Majaron and Lukac that accounted for ablation front inclination [22]. These craters are well demarcated with a tapered profile from the calculus surface to the crater base. The OCT crater images support the suggestion that pulsed laser ablation using infrared lasers with a pulse duration greater than 1 μs, is predominantly photothermal [9], [20]. The crater shape (Fig. 7) is uncharacteristic of photomechanical or photoacoustical interactions [7], [35], which often exhibit irregular surfaces due to large fragment dissociation and fractures.

Photothermal ablation of hard tissue in the infrared spectrum is evidenced by melting and recrystalization of particles [8], chemical decomposition [38], and stress due to rapid heating [10]. In a previous FEL calculus ablation study, we reported thermal damage (charred layer $\sim$20 μm) around a cystine crater when the repetition rate was increased to 15 Hz for a total of 25 pulses at 2.12-μm [39]. When the firing rate is increased and total irradiation time extended beyond the thermal relaxation time, sufficient heat is transferred beyond the volume of direct light absorption to carbonize the sides of the crater.

The effect of individual micropulses (1 ps) in the FEL macropulse (3–5 μs) on stress generation in the irradiated volume is inconclusive [10]. No acoustic measurement is known to us that could temporally resolve the FEL micropulse train-induced acoustic transients. Therefore, the potential contributions of micropulse-induced photomechanical damage in this experiment is not known. Fig. 8(a)(iii) and (c)(iii) show that fractures occurred surrounding the ablation crater surface for uric acid and cystine calculi with striated formation or with porous structures when the wavelengths selected coincide with relatively high optical absorptions (absolute absorption coefficients unknown). It is possible that the FEL micropulses accumulate mechanical stresses with a sharper pressure gradient within the optical penetration depth at higher absorption coefficients. Therefore, at higher optical absorptions, the micropulses may affect the ablation process in the calculus. In fact, a theoretical study by Uhlhorn where the pressure transients due to individual FEL micropulses were calculated using a hydrodynamic code (LATIS-3D), indicate that even though the absolute pressures are small, pressure gradients as high as 800 bar/μm are expected to be generated by individual FEL micropulses [40]. However, in the present study, photomechanical disruptions did not result in gross detachment of the calculi beyond the irradiated areas. No fracture was observed in COM calculi for all the laser wavelengths we used. This is not surprising given that the COM calculus is known to be the harder calculus type among typical urinary calculi [41].

Overall, results indicated that optimal wavelengths for ablation occurred at the 3-μm and 6-μm high absorption bands for most urinary calculi examined (Fig. 6), as previously suggested by Daidoh *et al.* [19] for uric acid and COM calculi. The agreement of the experimental threshold fluence and ablation depth data with the photothermal model indicates that in laser lithotripsy, unlike bone ablation recently reported by Peavy *et*

al. using the FEL, the laser wavelengths may be chosen based upon the mean optical absorption spectrum of the calculus and not the chromophores-specific absorption spectra [42]. Interestingly, Peavy *et al.* concluded that in bone ablation, if any chromophores (i.e., water and hydroxyapatites) other than type-I collagen were targeted, the mechanical strength of the collagen resisted the removal of tissue even though destruction of the other constituents occurred.

From the standpoint of clinical application, the markedly lower threshold fluences and higher ablation depths around the 3-μm absorption peak compared to other wavelengths implicated the potential of the Er : YAG laser, which produces radiation at 2.94 μm. It can be seen from Fig. 4 that the threshold fluences at 2.94 μm are 5.6 times lower for cystine calculus, 15.7 times lower for COM calculus, and 20.8 times lower for uric acid calculus as compared to those at 2.12 μm. Meanwhile, the ablation depths at 2.94 μm are 1.2 times higher for uric acid calculus, 2.9 times higher for COM calculus, and 1.7 times higher for cystine as compared to those at 2.12 μm, the wavelength of the Ho : YAG laser, as shown in Fig. 6. If the Er : YAG laser is operated at comparable pulse durations (i.e., 200–300 μs) to that of the Ho : YAG laser in clinical laser lithotripsy, it may be a reasonable assumption that similar trends or results in the threshold fluences and ablation depths are expected.

Since clinical laser lithotripsy is performed in a saline environment, the dynamics of ablation under water for these wavelengths must be considered [43]. An *in vitro* study in water shows that the Er : YAG laser lithotripsy is more efficient than the Ho : YAG laser lithotripsy for the COM calculus [44], [45], supported by the fact that water absorption and typical absorptions for common human calculi are higher at 2.94 μm than they are at 2.12 μm. However, the clinical use of infrared laser radiation at 6 μm is at the present time not ready for widespread use in a clinical setting. Clearly, the use of the FEL for medical applications, due to cost, space, and technical issues, is limited to few unique facilities. No commercially available or affordable 6-μm laser for clinical applications is known to the authors. However, recent technological advances indicate that novel solid-state devices such as an OPO may become available in the near future that are amenable to clinical ablation purposes. Moreover, light delivery in this spectral band can now be accomplished by hollow waveguides [33], [46]–[49] or fiber optic materials such as chalcogenide [50] or silver halide [51], [52], thus allowing delivery of pulsed laser radiation in a noninvasive catheter-based fashion. Although no clinical endoscopic use of such fibers is known in surgical urology, research activities are emerging in this area. For instance, an *in vitro* investigation of Er : YAG laser lithotripsy using sapphire fibers has been performed, yielding very promising results that warranted further *in vivo* studies [45], [53], [54].

V. Conclusion

We have demonstrated in this study that the ablation process is highly dependent upon optical absorption. The threshold fluence for ablation of urinary calculi is inversely proportional to the absorption coefficient. The ablation mechanism exhibited by the free electron laser ($\tau_p = 3$–5 μs) in the infrared is predominantly photothermal, although results indicated that other mechanisms such as photomechanical disruptions might be involved. Given *a priori* knowledge of laser–tissue interaction processes and physical properties such as the absorption coefficients, the optimal wavelengths may be selected for infrared laser ablation or fragmentation of urinary calculi.

References

[1] S. P. Dretler, "Laser lithotripsy: A review of 20 years of research and clinical applications," *Lasers Surg. Med.*, vol. 8, pp. 341–356, 1988.

[2] G. Watson, "The pulsed dye laser for urinary calculi in 600 patients," *SPIE Proc.*, vol. 1200, pp. 66–71, 1990.

[3] G. Watson, S. Murray, S. P. Dretler, and J. A. Parrish, "The pulsed dye laser for fragmenting urinary calculi," *J. Urol.*, vol. 138, pp. 195–198, 1987.

[4] G. M. Watson, S. L. Jacques, S. P. Dretler, and J. A. Parrish, "Tunable pulsed dye laser for fragmentation of urinary calculi," *Lasers Surg. Med.*, vol. 5, p. 160, 1985.

[5] P. Teng, N. S. Nishioka, W. A. Farinelli, R. R. Anderson, and T. F. Deutsch, "Microsecond-long flash photography of laser-induced ablation of biliary and urinary calculi," *Lasers Surg. Med.*, vol. 7, pp. 394–397, 1987.

[6] K. Rink, G. Delacretaz, and R. P. Salathe, "Fragmentation process induced by microsecond laser pulses during lithotripsy," *Appl. Phys. Lett.*, vol. 61, pp. 258–260, 1992.

[7] ——, "Fragmentation process of current laser lithotriptors," *Lasers Surg. Med.*, vol. 16, pp. 134–146, 1995.

[8] S. A. Schafer, F. M. Durville, B. Jassemnejad, K. E. Bartels, and R. C. Powell, "Mechanisms of biliary stone fragmentation using the Ho : YAG laser," *IEEE Trans. Biomed. Eng.*, vol. 41, pp. 276–283, 1994.

[9] K. F. Chan, G. J. Vassar, T. J. Pfefer, J. M. H. Teichman, R. D. Glickman, S. E. Weintraub, and A. J. Welch, "Holmium : YAG laser lithotripsy: A dominant photothermal ablative mechanism with chemical decomposition of urinary calculi," *Lasers Surg. Med.*, vol. 25, pp. 22–37, 1999.

[10] S. L. Jacques, "Laser–tissue interactions: Photochemical, photothermal, and photomechanical," *Lasers Gen. Surg.*, vol. 72, pp. 531–558, 1992.

[11] E. D. Jansen, T. Asshauer, M. Frenz, M. Motamedi, G. Delacretaz, and A. J. Welch, "Effect of pulse duration on bubble formation and laser-induced pressure waves during holmium laser ablation," *Lasers Surg. Med.*, vol. 18, pp. 278–293, 1996.

[12] J. A. Izatt, D. S. Norris, F. Partovi, M. Fitzmaurice, R. P. Rava, I. Itzkan, and M. Feld, "Ablation of calcified biological tissue using pulsed hydrogen fluoride laser radiation," *IEEE J. Quant. Electr.*, vol. 26, pp. 2261–2270, 1990.

[13] K. Nahen and A. Vogel, "Shielding by the ablation plume during Er : YAG laser ablation," *Laser–Tissue Interaction XII, SPIE Proc.*, vol. 4257, pp. 282–297, 2001.

[14] J. T. Walsh and J. P. Cummings, "Effect of the dynamic optical properties of water on midinfrared laser ablation," *Lasers Surg. Med.*, vol. 15, pp. 295–305, 1994.

[15] E. D. Jansen, T. G. van Leeuwen, M. Motamedi, C. Borst, and A. J. Welch, "Temperature dependency of the absorption coefficient of water for mid-infrared laser irradiation," *Lasers Surg. Med.*, vol. 14, pp. 258–264, 1994.

[16] J. T. Walsh and T. F. Deutsch, "Pulsed CO2 laser ablation of tissue: Effect of mechanical properties," *IEEE Trans. Biomed. Eng.*, vol. 36, pp. 1195–1201, 1989.

[17] R. P. Godwin and E. J. Chapyak, "Laser mass ablation efficiency measurements indicate bubble-driven dynamics dominates laser thrombolysis," *SPIE Proc.*, vol. 3245, pp. 4–11, 1998.

[18] E. D. Jansen, T. Asshauer, M. Frenz, G. Delacretaz, M. Motamedi, and A. J. Welch, "Effect of Young's modulus on bubble formation and pressure waves during pulsed holmium ablation of tissue phantoms," *SPIE Proc.*, vol. 2391, pp. 386–392, 1995.

[19] Y. Daidoh, T. Arai, Y. Komine, K. Nagakura, K. Ieda, M. Murai, H. Nakamura, M. Nakagawa, M. Kikuchi, M. Uchibori, S. Inazaki, and M. Wakaki, "Determination of optimum wavelength for laser photofragmentation of urinary stones," *J. Endourol.*, vol. 5, pp. 245–249, 1991.

[20] G. J. Vassar, J. M. H. Teichman, R. D. Glickman, S. E. Weintraub, K. F. Chan, T. J. Pfefer, and A. J. Welch, "Holmium : YAG lithotripsy: Photothermal mechanism," *J. Endourol.*, vol. 13, pp. 181–189, 1999.

[21] N. M. Wannop, M. R. Dickinson, and T. A. King, "Erbium : YAG laser radiation interaction with dental tissue," *SPIE Proc.*, vol. 2080, pp. 33–43, 1993.

[22] B. Majaron and M. Lukac, "Calculation of crater shape in pulsed laser ablation of hard tissues," *Lasers Surg. Med.*, vol. 24, pp. 55–60, 1999.
[23] A. Olmes, H. G. Franke, E. Bansch, H. Lubatschowski, M. Raible, G. Dziuk, and W. Ertmer, "Modeling of infrared soft-tissue photoablation process," *Appl. Phys. B*, vol. 65, pp. 659–666, 1997.
[24] T. G. van Leeuwen, E. D. Jansen, M. Motamedi, C. Borst, and A. J. Welch, "Pulsed laser ablation of soft tissue," in *Optical-Thermal Response of Laser-Irradiated Tissue*, A. J. Welch and M. J. C. van Gemert, Eds. New York: Plenum, 1995, pp. 709–763.
[25] R. Hibst and U. Keller, "Experimental studies of the application of the Er : YAG laser on dental hard substances: I. Measurement of the ablation rate," *Lasers Surg. Med.*, vol. 9, pp. 338–344, 1989.
[26] M. Ostertag, J. T. McKinley, L. Reinisch, D. M. Harris, and N. H. Tolk, "Laser ablation as a function of the primary absorber in dentin," *Lasers Surg. Med.*, vol. 21, pp. 384–394, 1997.
[27] J. T. Walsh and T. F. Deutsch, "Er : YAG laser ablation of tissue: Measurement of ablation rates," *Lasers Surg. Med.*, vol. 9, pp. 327–337, 1989.
[28] K. F. Chan, "Pulsed infrared laser ablation and clinical applications," Ph.D. dissertation, Univ. of Texas, Austin, 2000.
[29] K. F. Chan and A. J. Welch, "Free electron laser ablation of urinary calculi: A theoretical review," Phys. Med. Biol., 2001, submitted for publication.
[30] J. A. Izatt, D. Albagli, I. Itzkan, and M. Feld, "Pulsed laser ablation of calcified tissue: physical mechanisms and fundamental parameters," *SPIE Proc.*, vol. 1202, pp. 133–140, 1990.
[31] N. Q. Dao and M. Daudon, *Infrared and Raman Spectra of Calculi*. Paris, France: Elsevier, 1997.
[32] J. M. Khosrofian and B. A. Garetz, "Measurement of a Gaussian laser beam diameter through the direct inversion of knife-edge data," *Appl. Opt.*, vol. 22, pp. 3406–3410, 1983.
[33] H. S. Pratisto, S. R. Uhlhorn, M. Copeland, and E. D. Jansen, "Clinical beam delivery of the Vanderbilt FEL: Design and performance of a hollow waveguide-based handheld probe for neurosurgery," *SPIE Proc.*, vol. 3596, pp. 55–61, 1999.
[34] C. P. Cain, G. D. Noojin, and L. Manning, "A comparison of various probit methods for analyzing yes/no data on a log scale," USAF Armstrong Lab., Tech. Rep. AL/OE-TR-1996-0102, 1996.
[35] K. M. Bhatta, "Lasers in urology," *Lasers Surg. Med.*, vol. 16, pp. 312–330, 1995.
[36] J. M. H. Teichman, G. J. Vassar, J. T. Bishoff, and G. C. Bellman, "Holmium : YAG lithotripsy yields smaller fragments than lithoclast, pulsed dye laser or electrohydraulic lithotripsy," *J. Urol.*, vol. 159, pp. 17–23, 1998.
[37] F. A. Duck, *Physical Properties of Tissue*: Academic, 1990, ch. 2.
[38] R. D. Glickman, J. M. H. Teichman, N. S. Corbin, G. J. Vassar, S. E. Weintraub, K. F. Chan, and A. J. Welch, "Photothermal ablation is the primary mechanism in Holmium : YAG laser lithotripsy of urinary calculi," *SPIE Proc.*, vol. 3863, pp. 376–384, 1999.
[39] K. F. Chan, D. X. Hammer, G. Vargas, B. Sorg, T. J. Pfefer, H. Pratisto, E. D. Jansen, J. M. H. Teichman, and A. J. Welch, "Free electron laser ablation of urinary calculi: A preliminary study," *J. Urol.*, vol. 161 (suppl.), p. 369 (abstract no. 1430), 1999.
[40] S. R. Uhlhorn, R. A. London, A. J. Makarewicz, and E. D. Jansen, "Hydrodynamic modeling of tissue ablation with free-electron laser," *Laser–Tissue Interaction XI, SPIE Proc.*, vol. 3914, pp. 238–243, 2000.
[41] H. A. Razvi, J. D. Denstedt, S. S. Chun, and J. L. Sales, "Intracorporeal lithotripsy with the holmium : YAG laser," *J. Urol.*, vol. 156, pp. 912–914, 1996.
[42] G. M. Peavy, L. Reinisch, J. T. Payne, and V. Venugopalan, "Comparison of cortical bone ablations by using infrared laser wavelengths 2.9 to 9.2μm," *Lasers Surg. Med.*, vol. 26, pp. 421–434, 1999.
[43] M. Frenz, H. Pratisto, F. Konz, E. D. Jansen, A. J. Welch, and H. P. Weber, "Comparison of the effects of absorption coefficient and pulse duration of 2.12-μm and 2.79-μm radiation on laser ablation of tissue," *IEEE J. Quant. Electron.*, vol. 32, pp. 2025–2036, 1996.
[44] K. F. Chan, J. M. H. Teichman, P. J. Parker, R. D. Glickman, and A. J. Welch, "Erbium : YAG vs. Holmium : YAG lithotripsy," presented at the AUA, Apr. 28–May 2 2000.
[45] J. M. H. Teichman, K. F. Chan, P. P. Cecconi, A. Kamerer, N. S. Corbin, and A. J. Welch, "Erbium : YAG versus Holmium : YAG lithotripsy," *J. Urol.*, vol. 165, pp. 876–79, 2001.
[46] H. S. Pratisto, S. R. Uhlhorn, and E. D. Jansen, "Beam delivery of the Vanderbilt Free Electron Laser with hollow wave guides: effect on temporal and spatial pulse propagation," *Fiber Integrat. Opt.*, vol. 20, pp. 83–94, 2000.
[47] Y. Matsuura, K. Matsuura, and J. A. H. , "Power delivery of free electron laser light by hollow glass waveguides.," *Appl. Opt.*, vol. 35, pp. 5395–5397, 1996.
[48] I. Gannot, A. Inberg, M. Oksman, R. Waynant, and N. Croitoru, "Current status of flexible waveguides for IR laser radiation transmission," *IEEE J. Select. Topics Quant. Electron.*, vol. 2, pp. 880–889, 1996.
[49] I. Gannot, R. Waynant, A. Inberg, and N. Croitoru, "Broadband flexible waveguides for free-electron laser radiation," *Appl. Opt.*, vol. 36, pp. 6289–6293, 1997.
[50] J. S. Sanghera, L. B. Shaw, L. E. Busse, D. Talley, and I. D. Aggarwal, "Infrared transmitting fiber optics for biomedical applications," *SPIE Proc.*, vol. 3596, pp. 178–181, 1999.
[51] F. Moser, D. Bunimovich, A. DeRowe, O. Eyal, A. German, Y. Gotshal, A. Levite, L. Nagli, A. Ravid, V. Scharf, S. Shalem, D. Shemesh, R. Simchi, I. Vasserman, and A. Katzir, "Medical applications of infrared transmitting silver halide fibers," *IEEE J. Select. Topics Quant. Electron.*, vol. 2, pp. 872–879, 1996.
[52] L. Nagli, D. Bunimovich, A. Shmilevich, N. Kristianpoller, and A. Katzir, "Optical properties of mixed silver halide crystals and fibers," *Appl. Phys.*, vol. 74, pp. 5737–5741, 1993.
[53] K. F. Chan, G. Vargas, P. J. Parker, J. M. H. Teichman, R. D. Glickman, H. S. McGuff, and A. J. Welch, "*In vitro* Er : YAG laser lithotripsy," *SPIE Proc.*, vol. 3914, pp. 198–206, 2000.
[54] K. F. Chan, H. Lee, G. Vargas, J. M. H. Teichman, A. Kamerer, H. S. McGuff, and A. J. Welch, "Erbium : YAG Laser lithotripsy mechanism," J. Urol., Oct. 2001, submitted for publication.

Kin Foong Chan (S'92–M'00) was born in Penang, Malaysia, on December 22, 1973. He received the B.S., M.S., and Ph.D. degrees in electrical engineering from the University of Texas at Austin in 1996, 1997, and 2000, respectively.

Between 1994 and 1998, he was an Electronics Coop and Engineer at National Instruments Corporation in Austin, TX. Since 2000, he has been an Optical Research Engineer with Ball Semiconductor, Inc., Dallas, TX. His research interests include biomedical optics and instrumentation, optical MEMs, electro-optical devices, microlithography, and optical nanotechnology. He has published 15 journal and proceedings articles in laser–tissue interactions, and has eleven U.S. patents pending in other photonic areas.

Dr. Chan is a member of Tau Beta Pi, Eta Kappa Nu, and the SPIE.

Bernard Choi was born in Chicago, IL, on September 3, 1974. He received the B.S. degree from Northwestern University, Evanston, IL, in 1996 and the M.S. and Ph.D. degrees from the University of Texas at Austin in 1998 and 2001, respectively, all in biomedical engineering.

He is currently working as Postdoctoral Fellow at the Beckman Laser Institute, University of California, Irvine. His research interests include medical applications of infrared detectors, therapeutic applications of lasers in dermatology, and optical-thermal numerical modeling.

Gracie Vargas received the B.A. degree in physics from Gustavus Adolphus College, St. Peter, MN, in 1994. She received the M.S. degree in mechanical engineering in 1997 and the Ph.D. degree in biomedical engineering in 2001 from the University of Texas at Austin.

She is currently a Postdoctoral Fellow at the Biomedical Engineering Laser Laboratory at the University of Texas at Austin. Her research includes the reduction of light scattering in biological tissue for the improvement of light diagnostic and therapeutic techniques, the use of optical coherence tomography for diagnostic procedures, and the laser treatment of cutaneous vascular lesions.

Daniel X. Hammer (M'01) received the B.S. degree in electrical engineering from Rensselaer Polytechnic Institute, Troy, NY, in 1991 and the M.S. and Ph.D. degrees in electrical engineering from the University of Texas at Austin in 1998 and 2001, respectively. His Ph.D. dissertation work involved infrared sensitivity of the pyrophilic beetle, Melanophila acuminata.

From 1992 to 1996, he was stationed at Brooks AFB, San Antonio, TX, where he performed research on nonlinear optical phenomena associated with ultrashort laser pulses interaction with biological media. In 2001, he joined the technical staff of Physical Sciences Inc., Andover, MA, as a Principal Scientist. His research interests include white-light interferometry, thermal denaturation, laser lithotripsy, laser-induced cavitation bubbles, confocal imaging of blood vessels, and laser tissue soldering ophthalmic imaging, medical instrumentation, and low-coherence interferometry.

He is a member of the Optical Society of America and the Society of Photo-Optical Instrumentation Engineers.

Brian Sorg received the B.S. degree in electrical engineering from the University of Maryland, Baltimore, the M.S. degree in biomedical engineering from The Johns Hopkins University, Baltimore, and the Ph.D. degree in biomedical engineering from the University of Texas at Austin.

He is currently a Postdoctoral Research Associate at Duke University Medical Center, Durham, NC, in the Radiation Oncology Department. His research interests include therapeutic and diagnostic uses of optics and lasers.

Dr. Sorg is a member of Tau Beta Pi and Phi Kappa Phi.

T. Joshua Pfefer received the B.S. degree in mechanical engineering from Northwestern University, Evanston, IL, in 1991, and the M.S. degree in mechanical engineering and the Ph.D. degree in biomedical engineering from the University of Texas at Austin in 1993 and 1999, respectively.

He spent a year as a Research Fellow at the Wellman Laboratories of Photomedicine, Massachusetts General Hospital, studying applications of fluorescence spectroscopy in gastroenterology, and is presently an ORISE Postdoctoral Fellow at the Center for Devices and Radiological Health, U.S. Food and Drug Administration, Rockville, MD. His research interests include fluorescence and reflectance spectroscopy, pulsed laser-tissue interactions, and optical-thermal numerical modeling.

Joel M. H. Teichman received the S.B. degree in applied biology from the Massachusetts Institute of Technology, Cambridge, in 1983 and the M.D. degree from McGill University, Montreal, PQ, in 1987. He completed his urology residency training at the University of California at San Diego in 1993 and a fellowship in endourology at the University of Minnesota, Minneapolis, in 1994.

He is currently an Associate Professor in the Division of Urology at the University of Texas Health Science Center, San Antonio, TX, where he serves as the Head of the Section Endourology. His main research activities are focused on endourology and laser lithotripsy.

Ashley J. Welch received the B.E. degree in electrical engineering from Texas Tech University, Austin, in 1955, the M.S. degree in electrical engineering from Southern Methodist University, Dallas, TX, in 1959, and the Ph.D. degree in electrical engineering from Rice University, Houston, TX, in 1964.

He is currently Professor of Electrical and Computer Engineering and Biomedical Engineering and is the Marion E. Forsman Centennial Professor of Engineering at the University of Texas at Austin. He joined the University of Texas at Austin as an Assistant Professor in 1964. He is an international authority on the optical and thermal response of tissue to laser irradiation. His current recent interests include, fundamental analysis of laser–tissue interaction, OCT imaging, and feedback control to physically describe and enhance laser treatment of port wine stain, tissue welding, and skin resurfacing. He has published over 225 papers and book chapters describing his research.

E. Duco Jansen was born in Epe, The Netherlands, in 1966. He received the Drs. (M.S.) degree in medical biology from the University of Utrecht, The Netherlands, in 1990 and the M.S. and Ph.D. degrees in biomedical engineering from the University of Texas at Austin in 1992 and 1994, respectively.

Following a two-year post-doctoral appointment, he joined the faculty of the Department of Biomedical Engineering as Assistant Professor at Vanderbilt University, Nashville, TN, in 1997. His current research interests include medical applications of the Free Electron Laser, mechanisms of pulse laser ablation of biological tissue, noninvasive optical imaging of tissue ultrastructure, and cellular processes (gene expression).